Epithelial *Cdc42* Deletion Induced Enamel Organ Defects and Cystogenesis

Journal of Dental Research
2018, Vol. 97(12) 1346–1354

DOI: 10.1177/0022034518779546
journals.sagepub.com/home/jdr

J. Zheng[1,2,3*], X. Nie[2*], L. He[2], A.J. Yoon[4], L. Wu[1,3], X. Zhang[5], M. Vats[2], M.D. Schiff[2], L. Xiang[1,2,3], Z. Tian[2], J. Ling[1], and J.J. Mao[1,2,6,7]

Abstract

Cdc42, a Rho family small GTPase, regulates cytoskeleton organization, vesicle trafficking, and other cellular processes in development and homeostasis. However, Cdc42's roles in prenatal tooth development remain elusive. Here, we investigated Cdc42 functions in mouse enamel organ. Cdc42 showed highly dynamic temporospatial patterns in the developing enamel organ, with robust expression in the outer enamel epithelium, stellate reticulum (SR), and stratum intermedium layers. Strikingly, epithelium-specific *Cdc42* deletion resulted in cystic lesions in the enamel organ. Cystic lesions were first noted at embryonic day 15.5 and progressively enlarged during gestation. At birth, cystic lesions occupied the bulk of the entire enamel organ, with intracystic erythrocyte accumulation. Ameloblast differentiation was retarded upon epithelial *Cdc42* deletion. Apoptosis occurred in the *Cdc42* mutant enamel organ prior to and synchronously with cystogenesis. Transmission electron microscopy examination showed disrupted actin assemblies, aberrant desmosomes, and significantly fewer cell junctions in the SR cells of *Cdc42* mutants than littermate controls. Autophagosomes were present in the SR cells of *Cdc42* mutants relative to the virtual absence of autophagosome in the SR cells of littermate controls. Epithelium-specific *Cdc42* deletion attenuated Wnt/β-catenin and Shh signaling in dental epithelium and induced aberrant Sox2 expression in the secondary enamel knot. These findings suggest that excessive cell death and disrupted cell-cell connections may be among multiple factors responsible for the observed cystic lesions in *Cdc42* mutant enamel organs. Taken together, *Cdc42* exerts multidimensional and pivotal roles in enamel organ development and is particularly required for cell survival and tooth morphogenesis.

Keywords: cell death, cysts, Rho GTPase, odontogenesis, Wnt signaling pathway, tooth germ

Introduction

Tooth development is initiated by the formation of the dental placode, which is an epithelial thickening that interacts with neural crest–derived dental mesenchyme to form a tooth organ. Epithelium-mesenchyme interactions are crucial for tooth morphogenesis (Mao and Prockop 2012; Thesleff 2014; Jiang et al. 2017). Specifically for the developing enamel organ, a single-layer epithelium develops into not only the outer enamel epithelium and inner enamel epithelium (IEE) but also the centrally located cells, including cells of the stellate reticulum (SR) and stratum intermedium (SI; Thesleff and Tummers 2008). Much attention has been appropriately paid toward the development of IEE, which borders and interacts with the condensing mesenchyme and differentiates into enamel-forming ameloblasts (Peters and Balling 1999). However, the SR and SI cells, which are commonly viewed as supporting cells for the developing dental epithelium, have been less frequently studied (Thesleff and Tummers 2008; Liu et al. 2016; Regezi et al. 2016).

The Rho GTPase family plays increasingly recognized roles in tooth development (Li et al. 2016). Rho family GTPases, including RhoA, Rac1, and Cdc42, are expressed in the developing tooth organ and mediate the differentiation of ameloblasts and odontoblasts (Biz et al. 2010). Compared with RhoA and Rac1, Cdc42 functions in tooth development are poorly understood. In homeostasis, Cdc42 mediates signals of tyrosine kinase receptors, G protein–coupled receptors, and integrins through multiple signaling pathways and in multiple organ systems (Rul et al. 2002; Brunton et al. 2004). Cdc42 regulates multiple cellular processes, including cytoskeleton

[1]Guanghua School of Stomatology, Hospital of Stomatology, Sun Yat-sen University, Guangzhou, China
[2]Center for Craniofacial Regeneration, Columbia University, New York, NY, USA
[3]Department of Orthodontics, Hospital of Stomatology, Sun Yat-sen University, Guangzhou, China
[4]Oral and Maxillofacial Pathology Division, College of Dental Medicine, Columbia University, New York, NY, USA
[5]Departments of Ophthalmology, Pathology, and Cell Biology, Columbia University, New York, NY, USA
[6]Department of Pathology and Cell Biology, College of Physicians and Surgeons, Columbia University, New York, NY, USA
[7]Department of Orthopedic Surgery, College of Physicians and Surgeons, Columbia University, New York, NY, USA
*Authors contributing equally to this article.

A supplemental appendix to this article is available online.

Corresponding Author:
J.J. Mao, Columbia University, 630 W. 168 St., VC12-211, New York, NY 10032, USA.
Email: jmao@columbia.edu

dynamics, vesicle trafficking, and cell survival (Olson et al. 1995; Melendez et al. 2011). Global *Cdc42*-knockout mice die around embryonic day 5.5 (E5.5) (Chen et al. 2000). Tissue-specific *Cdc42* knockout in the heart, nervous system, liver, eyes, and other organs disrupts multiple developmental processes and organ functions (Melendez et al. 2011). In a recent report, inducible epithelium-specific *Cdc42* deletion was shown to disrupt YAP transnucleation in the incisor cervical loop of postnatal mice (Hu et al. 2017). However, *Cdc42* functions for prenatal tooth development remain elusive. Here, we demonstrate that epithelium-specific *Cdc42* deletion induced excessive apoptosis and cystic lesions in the enamel organ, suggesting its vital roles in tooth development.

Materials and Methods

Generation of Epithelium-Specific Cdc42*-Knockout Mice*

Animal research was approved by Columbia University Institutional Animal Care and Use Committee. *K14-cre* and $Cdc42^{loxp/loxp}$ mice were acquired from the Jackson Laboratory (Dassule et al. 2000; Chen et al. 2006). *K14-cre;* $Cdc42^{loxp/+}$ mice were established by crossing *K14-cre* mice with $Cdc42^{loxp/loxp}$ mice. The compound heterozygous mice were healthy and survived. *K14-cre;* $Cdc42^{loxp/loxp}$ ($Cdc42^{cKO}$) mutant mice were generated by crossing *K14-cre;* $Cdc42^{loxp/+}$ mice with $Cdc42^{loxp/loxp}$ mice. Mouse genotyping was performed by general polymerase chain reaction (PCR) with the *Cdc42* primer (F5′-AG ACAAAACAACAAGGTCCAGA-3′; R5′-GCACCATCACC AACAACAAC-3′) per genotyping protocol from the Jackson Laboratory.

Gross Examination, Histology, Immunofluorescence, and Confocal Microscopy

Gross examination was performed under a stereomicroscope (SMZ800; Nikon). Tooth organs were decalcified with 0.5M ethylenediaminetetraacetic acid (EDTA) as needed, with paraffin blocks sectioned at 5-μm thickness. Frontal sections were used unless otherwise stated. For immunofluorescence, heat-based antigen retrieval was applied. The following antibodies were used: Cdc42 (ab187643; Abcam), pan-keratin (ab8068; Abcam), laminin (ab11575; Abcam), β-catenin (ab32572; Abcam), ZO-1 (61-7300; Life Technologies), E-cadherin (ab76055; Abcam), Sox2 (ab97959; Abcam), amelogenin (sc365284; Santa Cruz), and ameloblastin (sc50534; Santa Cruz). Alexa Fluor secondary antibodies (A32732 or A32723; Invitrogen) were used for signal detection. Sections were examined with a Leica microscope (DM5000 B) and a Nikon confocal microscope (Orange A1RMP).

Organ Culture and Trichrome Staining

E14.5 mandibular first molar tooth germs were isolated and cultured in Transwell inserts in 12-well plates per our prior methods (Jiang et al. 2017) with Dulbecco's modified Eagle medium (DMEM) containing 10% heat-activated fetal bovine serum, 1% antibiotics, 1% GlutaMax, and 100μM ascorbic acid, and media were changed every other day. Tooth germs were processed for quantitative real-time PCR (qRT-PCR) and trichrome staining following 7- and 21-d culture.

Apoptosis and Proliferation Assays

TUNEL staining was performed with the DeadEnd TUNEL System (Promega) per the manufacturer's protocol. Immunofluorescence for phospho histone H3 (Millipore) was used for cell proliferation assay. Sections were cut per published protocols (Peterkova et al. 1996). We used serial sections of 3 independent samples at 10-μm intervals for E13.5, 20 μm for E14.5, and 30 μm for E15.5 tooth organs to quantify apoptosis and mitosis in the enamel organ (ImageJ).

Western Blot

Tissue lysates were prepared from isolated E15.5 tooth germs. Dental epithelium was separated from dental mesenchyme by Dispase I (Gibco) digestion, followed by dental epithelium homogenizing and lysing with radioimmunoprecipitation assay (RIPA) buffer for 30 min on ice, and centrifugation at 12,000 rpm for 20 min. Supernatants were used for Western blot, with protein concentrations determined by BCA kit (23225; Thermo Fisher Scientific). Approximately 10-μg proteins were loaded per lane. Cdc42 (ab187643; Abcam) and Gapdh (sc25778; Santa Cruz) antibodies were used. Secondary antibodies were dye labeled and detected with the Odyssey Infrared Imager system.

qRT-PCR

Total RNA was extracted by the RNeasy Microarray Tissue Mini Kit (QIAGEN) per the manufacturer's protocol. Dental epithelia isolated from E13.5, E14.5, E15.5, and postnatal day 0 (P0) and cultured tooth germs were treated with Dispase I. cDNA was synthesized with iScript cDNA Synthesis Kit (Bio-Rad). All primers were listed in Appendix Table. qRT-PCR was performed with the SYBR system (Bio-Rad). The $2^{-\Delta\Delta ct}$ method was used to measure the fold changes of *Cdc42, Lc3b, Lef1*, amelogenin (*Amelx*), and ameloblastin (*Ambn*), with *Gapdh* as a control.

Transmission Electron Microscopy

Tooth germs were isolated from E14.5 embryos, fixed with 2.5% glutaraldehyde for 2 h, and treated with 1% OsO4 in cacodylate buffer for 1 h. Following dehydration, tooth germs were embedded in Lx-112 (Ladd Research Industries). Thin sections were cut on the PT-XL ultramicrotome at 60-nm thickness and stained with uranyl acetate and lead citrate. Sections were examined with a JEOL JEM-1200 EXII transmission electron microscope. Images were captured with an ORCA-HR digital camera (Hamamatsu) and recorded with an AMT Image Capture Engine.

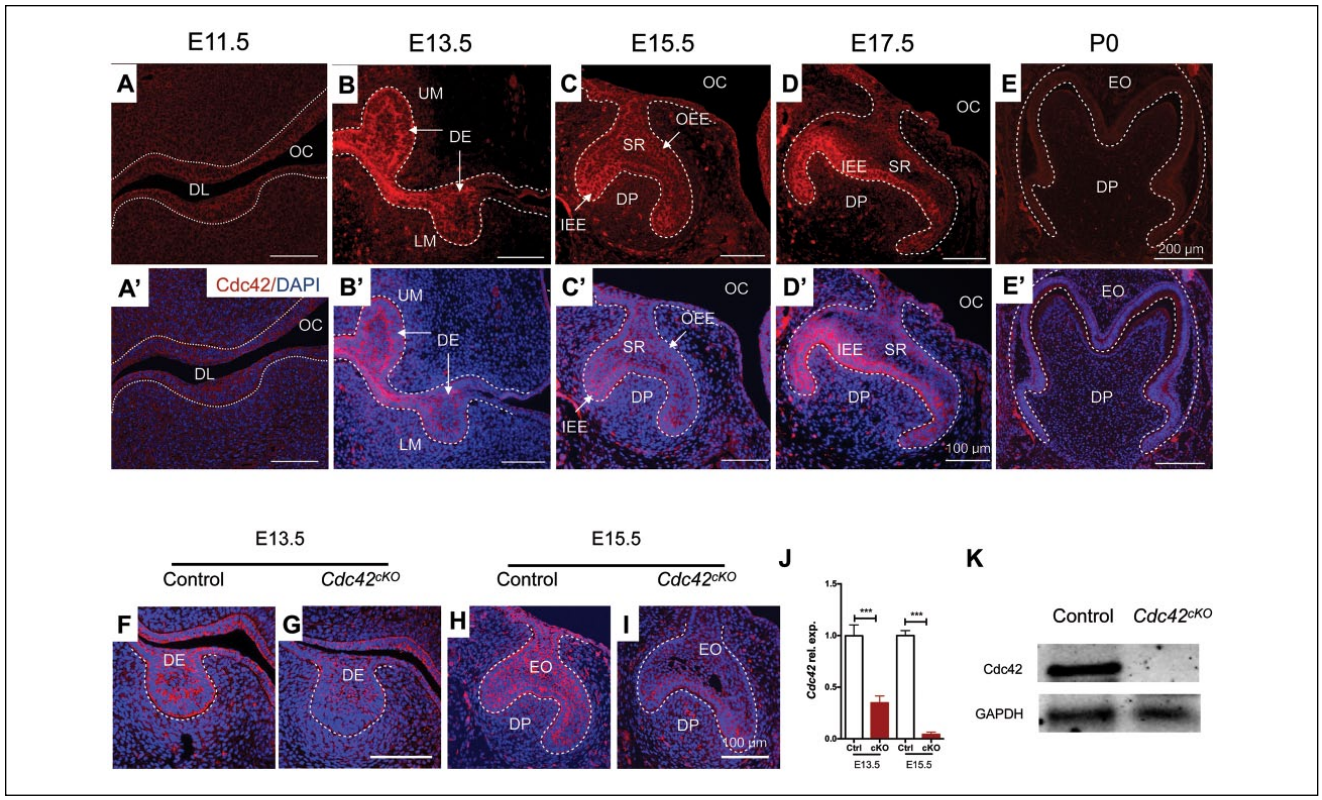

Figure 1. Cdc42 expression in developing tooth organ and generation of epithelium-specific *Cdc42* deletion mice. (**A–E**) Immunofluorescence of Cdc42 (red) at embryonic day 11.5 (E11.5), E13.5, E15.5, E17.5, and postnatal day 0 (P0). (**A′–E′**): Immunofluorescence of Cdc42 (red) overlaid with DAPI (blue). (**F–I**) Confocal microcopy images of control versus *K14-cre; Cdc42*$^{loxp/loxp}$ at E13.5 and E15.5. (A–I) Dotted lines indicate the epithelial compartment of the tooth germ. (**J**) Quantitative real-time polymerase chain reaction of *Cdc42* expression in the control and *K14-cre; Cdc42*$^{loxp/loxp}$ enamel organs at E13.5 and E15.5. Values are presented as mean ± SD. ***$P < 0.001$. (**K**) Western blot of Cdc42 expression in the control and *K14-cre; Cdc42*$^{loxp/loxp}$ enamel organs at E15.5. DE, dental epithelium; DL, dental lamina; DM, dental mesenchyme; DP, dental papilla; EO, enamel organ; IEE, inner enamel epithelium; LM, lower first molar; OC, oral cavity; OEE, outer enamel epithelium; SR, stellate reticulum; UM, upper first molar. Scale bars: 100 μm (A–D′, F–I), 200 μm (E, E′).

In Situ Hybridization

Sectional in situ hybridization was performed according to a predescribed method (Zhou et al. 2015). The *Shh* probe was generated by in vitro transcription of a plasmid construct (Gritli-Linde et al. 2002), with an in vitro transcription kit (MAXIscript T3/T7; Ambion).

Statistical Analysis

All experiments were performed in biological triplicates. All quantitative data were expressed as mean ± SD and analyzed by Student's *t* test or analysis of variance with Bonferroni tests upon confirmation of normal data distribution, with significance of $P < 0.05$.

Results

Cdc42 Expression in Tooth Development

We first mapped Cdc42 expression from E11.5 to P0 by immunofluorescence. Cdc42 was rather modest in the dental placode at E11.5 (Fig. 1A, A′). From E13.5 to E15.5, Cdc42 began robust expression in dental epithelium, including the IEE and newly formed SR layers (Fig. 1B–C′). Cdc42 further sustained a high level in the IEE and relatively weak expression in the SR and SI cells at E17.5 (Fig. 1D, D′). By P0, the Cdc42 level was substantially reduced (Fig. 1E, E′). In contrast, Cdc42 expression in dental mesenchyme was modest throughout the observed E11.5 and P0.

Epithelium-Specific Cdc42 *Deletion Yielded Cystic Lesions in the Enamel Organ*

Given Cdc42's remarkable expression pattern primarily in the developing dental epithelium, we generated *K14-cre; Cdc42*$^{loxp/loxp}$ mice to interrogate its putative functional roles in the developing enamel organ. The *K14-cre* mouse is a widely used cre strain with a high recombination efficiency (Dassule et al. 2000). To confirm that *K14-cre* induced epithelium-specific *Cdc42* deletion, we demonstrated diminished Cdc42 expression in E13.5 and E15.5 dental epithelia (Fig. 1G, I), relative to robust Cdc42 expression in the control tooth organs (Fig. 1F, H). qRT-PCR showed significantly less *Cdc42* mRNA in the

isolated dental epithelia of *K14-cre; Cdc42*$^{loxp/loxp}$ mice at E13.5 and E15.5 than littermate controls did (Fig. 1J), indicating successful *Cdc42* deletion. Western blot showed diminished Cdc42 in dental epithelia of tissue-specific *Cdc42* mutants at E15.5 as compared with littermate controls (Fig. 1K), indicating *Cdc42* deficiency at the protein level. *K14-cre; Cdc42*$^{loxp/loxp}$ mice died at P0, likely due to lethality of epithelium-specific *Cdc42* deletion, contrasting the death of global *Cdc42* mutant mice at E5.5 (Chen et al. 2000).

Importantly, *Cdc42* deletion caused cystic changes in the developing enamel organ. We first noted small empty cavities devoid of cells in the E15.5 enamel organ of *Cdc42* mutant mice as compared with controls (Fig. 2A, B). Immunofluorescence of laminin and pan-keratin showed a well-defined basement membrane and dental epithelium, within which small empty cavities formed with epithelium-specific *Cdc42* deletion (Fig. 2D) relative to controls (Fig. 2C). By E17.5, acellular cavities enlarged in the SR of *Cdc42*-deficient mice (Fig. 2F, H) relative to controls (Fig. 2E, G).

At P0, cystic lesions occupied the entire enamel organ, including the cervical loop, and were lined by flat epithelial cells with clear basement membranes, as indicated by laminin staining (Appendix Fig. 1, Fig. 2J), which are reminiscent of odontogenic cysts (Regezi et al. 2016). Gross examination of a representative developing molar sample at P0 showed substantially reduced crown size and diminished cusps in epithelium-specific *Cdc42* mutants (Fig. 2L, M) relative to a representative littermate control sample (Fig. 2K). Blood cells, likely derived from hemorrhage, filled in cyst cavities (Fig. 2M, O, O″), whereas no pathologic bleeding and irregular cystic lesions could be seen in the littermate control (Fig. 2K, N, N′, N″).

Impaired Ameloblast Differentiation upon Epithelium-Specific Cdc42 *Deletion*

Given the presence of cystic lesions in the developing enamel organ and direct expression of Cdc42 in the IEE, we further explored whether amelogenesis was negatively affected. We measured the thickness of the ameloblast layer per previously established methods (Jalali et al. 2017) and found that *Cdc42*-deficient mice showed significantly shorter ameloblast length than that of littermate controls (Fig. 2P). Furthermore, Amelx and Ambn as 2 key amelogenesis extracellular matrix proteins were decreased in *Cdc42* mutants at P0 as compared with controls (Fig. 2Q–T). qRT-PCR showed significantly reduced *Amelx* and *Ambn* mRNAs in *Cdc42* mutants than in controls (Fig. 2U).

To further appreciate amelogenesis, we isolated and cultured E14.5 tooth germs for up to 3 wk, also in consideration that epithelium-specific *Cdc42* deletion led to lethality at P0. In contrast to the continued development of control tooth germs in organ culture (Fig. 2V, X), *Cdc42* mutant tooth germs showed less pronounced enamel formation, as revealed by trichrome staining (Fig. 2W, Y). qRT-PCR of tooth germs, which were cultured for 7 d, revealed significantly reduced levels of *Amelx* and *Ambn*, suggesting that ameloblast differentiation defect was directly regulated by *Cdc42* disruption (Fig. 2Z). However, cystic changes may have contributed to defective ameloblast differentiation in mutants. In addition, the SI layer in *Cdc42* mutants was discontinuous and less abundant, as seen in hematoxylin and eosin sections (Fig. 2N′, O′) and pan-keratin-stained sections (Fig. 2I, J; Appendix Fig. 2).

Cdc42 *Deletion Induced Excessive Apoptosis in the Enamel Organ*

Given the formation of cystic lesions in *Cdc42* mutants, we assayed apoptosis of the developing tooth organs (Fig. 3, Appendix Fig. 3). TUNEL staining revealed an excessive number of apoptotic cells in mutant tooth bud starting from E13.5 (Fig. 3B), relative to the control (Fig. 3A, I). By E14.5, we consistently detected more vigorous apoptosis in the SR layer and the primary enamel knot (PEK) of the mutant than in the control (Fig. 3D, I; Appendix Fig. 3G–L). Remarkably, a dramatically increased number of apoptotic cells was seen in mutant PEKs as compared with stage-matched controls, suggesting excessive cell death in mutant PEKs. At E15.5, however, apoptosis in PEKs was no longer detectable in mutants, suggesting that excessive apoptosis had eliminated the majority of the PEK cells, if not all (Fig. 3F, I, red arrow; Appendix Fig. 1B3), as compared with the control (Fig. 3E, I, white arrow; Appendix Fig. 1A3). By E17.5 when empty cavities formed throughout the enamel organ, there was no longer pronounced cell death in the developing enamel organs of *Cdc42* mutants as opposed to controls (Fig. 3G–I).

To ensure that formation of cystic lesions in *Cdc42* mutants was not due to a hypothetical deficit in cell proliferation, we assayed mitosis by phospho histone H3 staining and found comparable cell proliferation ratios between *Cdc42*-knockout and control groups from E13.5 to E17.5 (Fig. 3J–P), suggesting that cell death, rather than cell proliferation deficit, was among probable causes of cystic change.

Epithelium-Specific Cdc42 *Deletion Disrupted Cell Junctions and Cytoskeleton Integrity and Activated Autophagy*

Given excessive cell death and the formation of cystic lesions in *Cdc42* mutants, we suspected that *Cdc42* deletion might have disrupted cell junctions and/or cytoskeleton. Transmission electron microscopy showed that SR cells were deficient of cell extensions in E14.5 enamel organs of *Cdc42* mutants, as compared with clearly identifiable cell extensions in controls (Fig. 4A, B). SR cells of *Cdc42* mutant enamel organs showed less abundant desmosomes and aberrant structures relative to controls (Fig. 4C, D). Quantitatively, cell junctions in the SR layer of *Cdc42* mutants were significantly fewer than controls (Fig. 4I). This observation was confirmed by reduced ZO-1 staining in mutants (Fig. 4E–H).

Actin filaments in *Cdc42* mutant desmosomes showed disrupted orientation relative to typical perpendicular patterns in controls (Fig. 4C, D). Aberrant actin filament assemblies were common in *Cdc42* mutant SR cells (Fig. 4J), suggesting defects

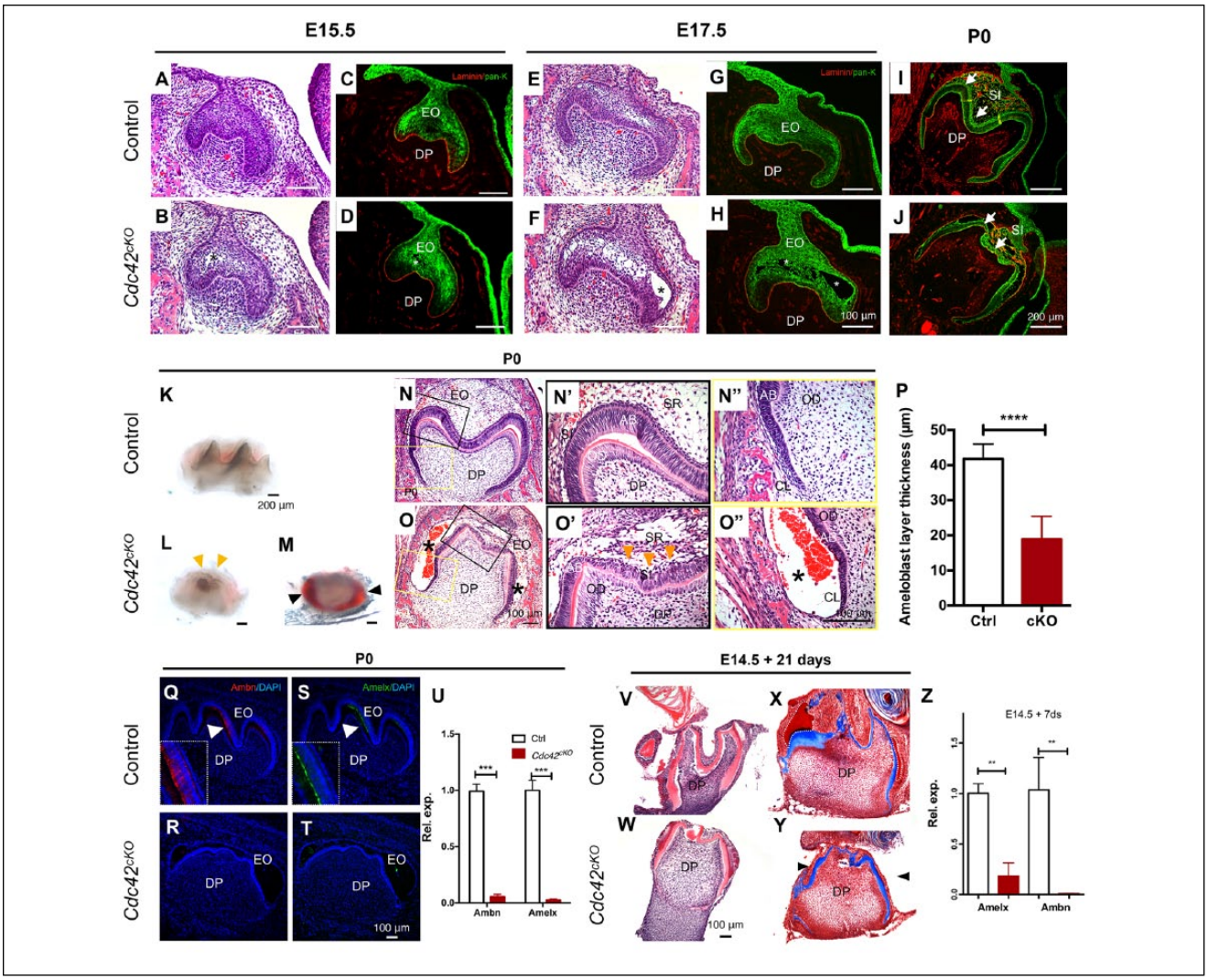

Figure 2. Epithelium-specific *Cdc42* deletion yielded cystic change and impaired ameloblast differentiation. (**A–D**) Hematoxylin and eosin (H&E) images of embryonic day 15.5 (E15.5) enamel organ and immunofluorescence of laminin (red) and pan-keratin (pan-k; green). Black asterisk in panel B indicates an emerging cavity in enamel organ. (**E–H**) H&E images of E17.5 enamel organ and immunofluorescence of laminin and pan-k. Asterisks in panels F and H indicate expanding cavity. (**I**, **J**) Immunofluorescence images of laminin and pan-k of postnatal day 0 (P0) enamel organs. White arrows show SI layers. (**K–M**) Dissection microscope images of molar tooth germs of control and *K14-cre; Cdc42*$^{loxp/loxp}$ (*Cdc42*^{cKO}) mutant. Yellow arrowheads indicate aberrant cusps; black arrowheads indicate cyst and hemorrhage. (**N**, **O**) H&E staining of the first molar tooth germ of control and *Cdc42*^{cKO} mice at P0. Fluid-filled cystic lesion (asterisk) with hemorrhage in panel O. (**N′**, **N″**, **O′**, **O″**) Magnified images from black and yellow frames in N and O; asterisks showing cystic changes, orange arrowheads showing disorganized SI cells and ameloblasts. (**P**) Quantification of ameloblast layer thickness at P0. Values are presented as mean ± SD. ****$P < 0.0001$. (**Q–T**) Immunofluorescence images of ameloblastin (Ambn; red), amelogenin (Amelx; green) and DAPI (blue) of control and *Cdc42*^{cKO} first molar tooth germs in the sagittal plane at P0. White arrowheads indicate positive expression in control samples. Inserts show positive staining in panels Q and S. (**U**) Quantitative real-time polymerase chain reaction (qRT-PCR) of *Ambn* and *Amelx* of dental epithelium isolated from control and *Cdc42*^{cKO} first molar tooth germs at P0. Values are presented as mean ± SD. ***$P < 0.001$. (**V**, **W**) H&E of tooth germs isolated from E14.5, followed by 21-d culture. (**X**, **Y**) Trichrome staining of tooth germs isolated from E14.5, followed by 21-d culture. Dashed-line areas indicate newly formed enamel in panel X; black arrowheads indicate newly formed enamel in panel Y. (**Z**) qRT-PCR of *Ambn* and *Amelx* of dental epithelium isolated from control and mutant E14.5 tooth germs, followed by 7-d culture. Values are presented as mean ± SD. **$P < 0.01$. AB, ameloblast; CL, cervical loop; DP, dental papilla; EO, enamel organ; OD, odontoblast; SI, stratum intermedium; SR, stellate reticulum. Scale bar: 100 µm (A–H, N–O″, Q–T, V–Y), 200 µm (I, J).

in cytoskeleton organization. However, E-cadherin immunofluorescence showed little difference between *Cdc42* mutants and controls (Appendix Fig. 2). Importantly, autophagosomes were present in the SR cells of *Cdc42* mutant enamel organs (Fig. 4K) relative to scarce autophagosomes in controls (Fig. 4A). qRT-PCR showed significantly higher levels of *Lc3b*, a marker for autophagosomes, in the enamel organs of *Cdc42* mutants than controls (Fig. 4N), suggesting that *Cdc42* deletion activated autophagy as another putative cause for excessive cell death. Additionally, *Cdc42* mutant IEE showed disarrayed cell orientations and increased cell-cell spaces (Figs. 1N′, O′ and 4L, M). *Cdc42* mutant mice further displayed

malformed basement membranes between ameloblasts and odontoblasts relative to controls (Fig. 4L, M).

Altered Molecular Signaling in Cdc42 *Mutant Enamel Organs*

To begin exploring molecular signaling pathways that might account for the observed dysmorphogenesis, autophagy, and cell death due to *Cdc42* deletion, we probed Wnt signaling for its previously demonstrated roles in cell survival and tooth morphogenesis (Liu and Millar 2010; O'Connell et al. 2012). There was marked attenuation of β-catenin, an intracellular mediator for canonical Wnt signaling, in mutant IEE and SR cells at E13.5, E15.5, and E17.5 (Fig. 5B, D, F) relative to controls (Fig. 5A, C, E). qRT-PCR showed that *Lef1*, a key mediator of canonical Wnt signaling, was significantly reduced in *Cdc42* mutants as compared with controls (Fig. 5G).

Sox2 is a progenitor cell marker in mouse molar development (Li et al. 2015) and regulates Wnt signaling during tooth development (Lee et al. 2016). Sox2 protein marked oral epithelium, lingual outer enamel epithelium, some SR and SI cells, and cells in the cervical loop, excluding secondary enamel knot (SEK) in the control enamel organ (Fig. 5H), consistent with previous studies (Zhang et al. 2012). Sox2 was consistently detected at mutant SEK at E17.5 (Fig. 5I), suggesting malformation of the SEK. In further support of this observation, levels of *Shh*, a critical signaling molecule for tooth morphogenesis (Dassule et al. 2000), was significantly reduced from SEK by in situ hybridization (Fig. 5J, K). Altogether, altered signaling and malformed SEK might explain the morphologic changes in mutants.

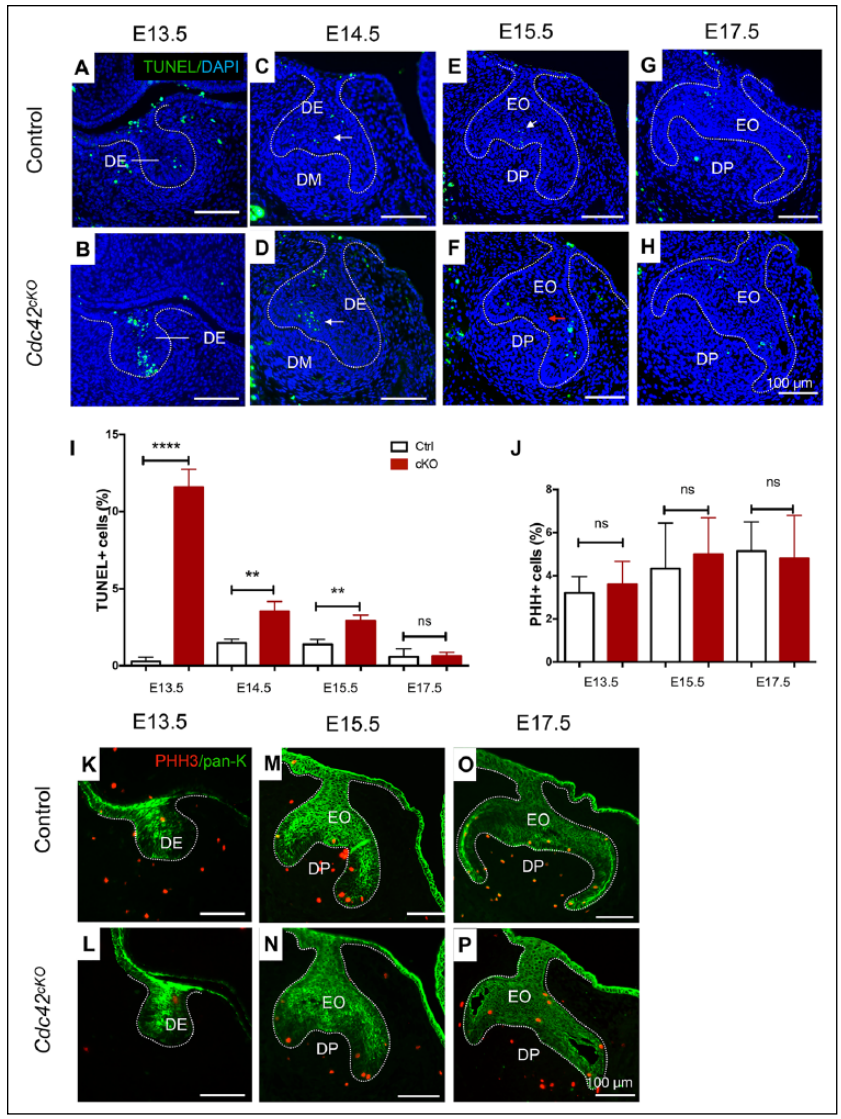

Figure 3. Epithelium-specific *Cdc42* deletion yielded excessive cell death in the developing enamel organ. (**A–H**) Representative TUNEL (green) images at embryonic day 13.5 (E13.5), E14.5, E15.5, and E17.5 tooth germs, overlaid with DAPI (blue). White arrows indicate primary enamel knot; red arrow indicates disappearance of primary enamel knot. Quantification of (**I**) TUNEL-positive cells and (**J**) phospho histone 3 (PHH3)–positive cells. Values are presented as mean ± SD. $^{**}P < 0.01$. $^{****}P < 0.0001$. (**K–P**) Representative PHH3 (red) immunofluorescence images of control and *Cdc42*^{cKO} enamel organs at E13.5, E15.5, and E17.5. (A–H, K–P) Dotted lines indicate the epithelial compartment of the tooth germ. DE, dental epithelium; DM, dental mesenchyme; DP, dental papilla; EO, enamel organ; ns, no significant difference. Scale bars: 100 μm.

Discussion

Cdc42 plays vital roles for enamel organ development. *Cdc42* deletion disrupts multiple cellular processes and induces cystic lesions in the developing enamel organ. Interestingly, cyst-like structures are present in the SR layer of the cervical loop in the incisor of 8-wk-old inducible *YAP/TAZ* mutant mice (Hu et al. 2017). Association of *Cdc42* mutations or abnormal activation with cystogenesis or other diseases was revealed in multiple organ systems (Modolo et al. 2012; Choi et al. 2013; Liu et al. 2013). Whether these cystic lesions are indeed odontogenic cysts requires additional studies. Our findings demonstrate that cyctic lesions in *Cdc42* mutant enamel organs are fluid-filled cavities with epithelium lining and a laminin-rich basement membrane. Actin disorganization in mutant SR cells suggests that Cdc42 regulates cytoskeleton integrity (Chen et al. 2000). Newly generated SR cells become star-shaped and form a network structure in the enamel organ through establishing cell junctions (Kallenbach 1978). Dysregulation of cytoskeleton in *Cdc42* mutants impairs cell-cell junctions and communications,

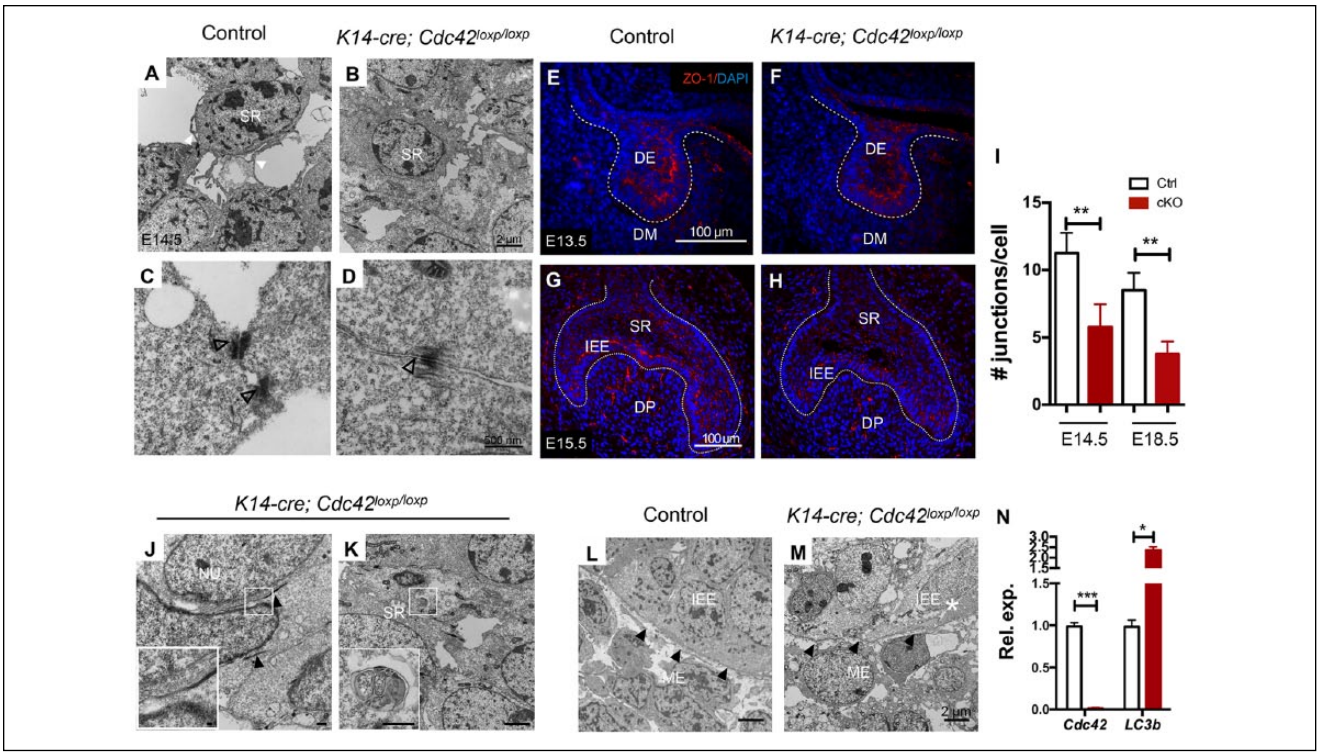

Figure 4. Epithelium-specific *Cdc42* deletion disrupted cell junctions and cytoskeleton and activated autophagy. Transmission electron microscope images of stellate reticulum (SR) cells at embryonic day 14.5 (E14.5) enamel organs in (**A**, **C**, **M**) controls and (**B**, **D**, **J**–**L**) *Cdc42* mutants. (A, B) Cell extension of SR cells. White arrowheads indicate cell extensions in E14.5 enamel organs. (C, D) Desmosomes in control and *Cdc42* mutant SR cells in E14.5 enamel organs. Black-border arrowheads indicate desmosomes. (**E–H**) ZO-1 (red) immunofluorescence in E13.5 and E15.5 enamel organs in control and *Cdc42* mutants. Dotted lines indicate the epithelial compartment of the tooth germ. (**I**) Quantification of cell-cell junction numbers per SR cell. Values are presented as mean ± SD. (J) Mutant SR cell. Black arrowheads indicate assemble actin filaments. (K) Autophagosomes in the SR cells in E14.5 enamel organs of the *Cdc42* mutant mice. White insert: magnified images of white squares. Inner enamel epithelium (IEE) in the (L) control and (**M**) *Cdc42* mutant mice. White asterisk indicates increasing cell-cell spaces among IEE. Black arrowheads indicate basement membrane. (**N**) Quantitative real-time polymerase chain reaction of *Cdc42* and *Lc3b* in E14.5 enamel organs. Values are presented as mean ± SD. DE, dental epithelium; DM, dental mesenchyme; DP, dental papilla; ME, mesenchyme; NU, nuclei. Scale bar: 2 μm (A, B, K, L, M), 500 nm (C, D; inset in K), 100 μm (E–H), 50 nm (J), 100 nm (insert in J). *$P < 0.05$. **$P < 0.01$. ***$P < 0.001$.

which may be among multiple causes for the observed cystic lesions.

Pronounced apoptosis in the PEK is considered necessary for the required disappearance of PEK at the late cap stage and early bell stage (Lesot et al. 1996; Shigemura et al. 2001). Here, we demonstrate *Cdc42*'s prosurvival roles in the enamel organ, as evidenced by excessive apoptosis in the mutants at the bud stage and early cap stage. Cdc42 is important for cell survival in multiple cell types and tissues, and its cleavage is likely a cause for apoptosis (Coleman and Olson 2002; Choi et al. 2013; Huang et al. 2016). The potential mechanisms for the apoptosis of SR cells in mutants are likely due to the defect in establishing cell-cell connections and actin dynamics, which produced survival signaling for the SR cells (Liu et al. 2016). However, the mechanisms by which *Cdc42* regulates PEK cells remain elusive. We speculate that excessive apoptosis in the *Cdc42* mutant enamel organ partially accounts for dysmorphogenesis and cystogenesis. Moreover, *Cdc42* deletion induces excessive autophagy (Yang et al. 2013; Booth et al. 2014). Putative connections, or the lack thereof, between autophagy and apoptosis warrants additional specific investigations.

In addition to the SR cells, ameloblast development is severely impaired by epithelium-specific *Cdc42* deletion, as evidenced by attenuated expression of ameloblastin and amelogenin, as well as reduced enamel formation by mutant ameloblasts in an organ culture system. This is consistent with the disrupted dental epithelium and ameloblast functions induced by other Rho GTPase inhibitors (Biz et al. 2010). The molecular mechanism of direct requirement of *Cdc42* for ameloblast differentiation remains to be elucidated. Reduced expression levels of β-catenin and *Lef1* in the IEE layer of mutant enamel organ suggest the impairment of the Wnt signaling pathway by *Cdc42* deletion and may explain abnormal ameloblast development. β-catenin augments Wnt signaling target genes by forming a transcription complex with Lef1 or by interaction with Tcf3 or Tcf4 (Cadigan and Waterman 2012). Attenuation of Shh signaling and aberrant Sox2 expression in the enamel organ of *Cdc42* mutants provide initial clues of complex molecular networks that are likely in place for *Cdc42* to regulate tooth organ development. Wnt and Shh signals are crucial for the survival of multiple cell types (Cobourne et al. 2001; Yang et al. 2006). Disruption of *Wnt* causes tooth development arrest at a very

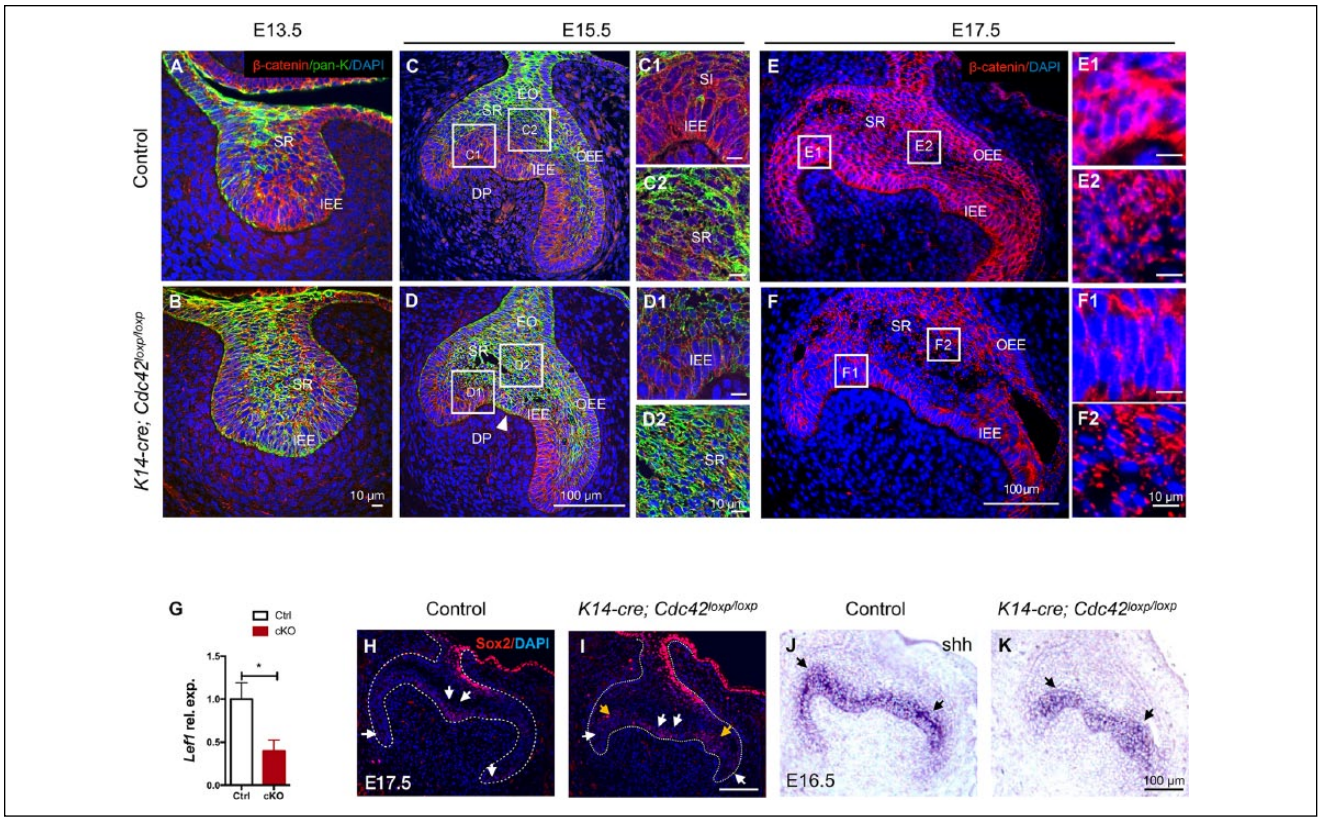

Figure 5. Disrupted signaling pathways in *Cdc42* mutant enamel organs. (**A–F**) Immunofluorescence of β-catenin (red), pan-keratin (green), and DAPI (blue) in embryonic day 13.5 (E13.5), E15.5, and E17.5 enamel organs. (C1, C2, D1, D2) Magnification of boxed areas in panels C and D, respectively. (E1, E2, F1, F2): Magnification of boxed areas in panels E and F, respectively. (**G**) Quantitative real-time polymerase chain reaction of *Lef1* in E15.5 enamel organs in control and *Cdc42* mutants. Values are presented as mean ± SD. **P* < 0.05. (**H**, **I**) Immunofluorescence of Sox2 (red) overlaid with DAPI (blue) at E17.5 control and *Cdc42* mutant enamel organs. White arrows indicate distribution of Sox2-positive cells. Yellow arrows indicate Sox2-positive cells in the secondary enamel knot in the mutant enamel organ. Dotted lines indicate the epithelial compartment of the tooth germ. (**J**, **K**) In situ hybridization of *shh* in E16.5 control and mutant enamel organs. Black arrows indicate secondary enamel knots. DP, dental papilla; EO, enamel organ; IEE, inner enamel epithelium; OEE, outer enamel epithelium; SI, stratum intermedium; SR, stellate reticulum. Scale bar: 10 μm (A, C1, C2, D1, D2, E1, E2, F1, F2), 100 μm (C, D, E, F, H–K).

early stage of tooth morphogenesis (Liu and Millar 2010). Shh is required for tooth growth and determines tooth morphology (Dassule et al. 2000). Attenuation of these critical signals might, at least in part, account for the differentiation defects and altered tooth morphogenesis in mutants. Additionally, ameloblast defects caused by *Cdc42* deletion could affect odontoblast development, which might further exaggerate ameloblast differentiation via impaired epithelial-mesenchymal interactions. Taken together, our findings suggest Cdc42's crucial roles in enamel organ development. Cdc42 is required for cytoskeleton dynamics, cell junction establishment, survival of SR cells, and proper differentiation of ameloblasts. Disruption of *Cdc42* may induce cystogenesis in the enamel organ and tooth malformation.

Author Contributions

J. Zheng, contributed to conception, design, data acquisition, analysis and interpretation, drafted the manuscript; X. Nie, contributed to conception, design, data collection and interpretation, critically revised the manuscript; L. He, A.J. Yoon, L. Wu, X. Zhang, M.D. Schiff, L. Xiang, Z. Tian, J. Ling, contributed to data analysis, critically revised the manuscript; M. Vats, contributed to data acquisition, critically revised the manuscript; J.J. Mao, contributed to conception, design, data analysis and interpretation, critically revised the manuscript. All authors gave final approval and agree to be accountable for all aspects of the work.

Acknowledgments

We thank Q. Guo, P. Ralph-Birkett, and Y. Tse for administrative and technical assistance. The work is supported by National Institutes of Health grants R01DE025643, R01DE023112, R01AR065023, and R01DE026297 to J. J. Mao and by the Guangdong Pioneer Grant (52000-52010002) and Guangdong Science and Technology Program (2016B030229003) to J.Q. Ling. The authors declare no potential conflicts of interest with respect to the authorship and/or publication of this article.

References

Biz MT, Marques MR, Crema VO, Moriscot AS, dos Santos MF. 2010. GTPases RhoA and Rac1 are important for amelogenin and DSPP

expression during differentiation of ameloblasts and odontoblasts. Cell Tissue Res. 340(3):459–470.
Booth LA, Tavallai S, Hamed HA, Cruickshanks N, Dent P. 2014. The role of cell signalling in the crosstalk between autophagy and apoptosis. Cell Signal. 26(3):549–555.
Brunton VG, MacPherson IR, Frame MC. 2004. Cell adhesion receptors, tyrosine kinases and actin modulators: a complex three-way circuitry. Biochim Biophys Acta. 1692(2–3):121–144.
Cadigan KM, Waterman ML. 2012. TCF/LEFs and Wnt signaling in the nucleus. Cold Spring Harb Perspect Biol. 4(11):a007906.
Chen F, Ma L, Parrini MC, Mao X, Lopez M, Wu C, Marks PW, Davidson L, Kwiatkowski DJ, Kirchhausen T, et al. 2000. Cdc42 is required for PIP(2)-induced actin polymerization and early development but not for cell viability. Curr Biol. 10(13):758–765.
Chen L, Liao G, Yang L, Campbell K, Nakafuku M, Kuan CY, Zheng Y. 2006. Cdc42 deficiency causes sonic hedgehog-independent holoprosencephaly. Proc Natl Acad Sci U S A. 103(44):16520–16525.
Choi SY, Chacon-Heszele MF, Huang L, McKenna S, Wilson FP, Zuo X, Lipschutz JH. 2013. Cdc42 deficiency causes ciliary abnormalities and cystic kidneys. J Am Soc Nephrol. 24(9):1435–1450.
Cobourne MT, Hardcastle Z, Sharpe PT. 2001. Sonic hedgehog regulates epithelial proliferation and cell survival in the developing tooth germ. J Dent Res. 80(11):1974–1979.
Coleman ML, Olson MF. 2002. Rho GTPase signalling pathways in the morphological changes associated with apoptosis. Cell Death Differ. 9(5):493–504.
Dassule HR, Lewis P, Bei M, Maas R, McMahon AP. 2000. Sonic hedgehog regulates growth and morphogenesis of the tooth. Development. 127(22):4775–4785.
Gritli-Linde A, Bei M, Maas R, Zhang XM, Linde A, McMahon AP. 2002. Shh signaling within the dental epithelium is necessary for cell proliferation, growth and polarization. Development. 129(23):5323–5337.
Hu JK, Du W, Shelton SJ, Oldham MC, DiPersio CM, Klein OD. 2017. An FAK-YAP-mTOR signaling axis regulates stem cell-based tissue renewal in mice. Cell Stem Cell. 21(1):91–106.e6.
Huang Z, Zhang L, Chen Y, Zhang H, Zhang Q, Li R, Ma J, Li Z, Yu C, Lai Y, et al. 2016. Cdc42 deficiency induces podocyte apoptosis by inhibiting the Nwasp/stress fibers/YAP pathway. Cell Death Dis. 7:e2142.
Jalali R, Lodder JC, Zandieh-Doulabi B, Micha D, Melvin JE, Catalan MA, Mansvelder HD, DenBesten P, Bronckers A. 2017. The role of Na:K:2Cl cotransporter 1 (NKCC1/SLC12A2) in dental epithelium during enamel formation in mice. Front Physiol. 8:924.
Jiang N, Xiang L, He L, Yang G, Zheng J, Wang C, Zhang Y, Wang S, Zhou Y, Sheu TJ, et al. 2017. Exosomes mediate epithelium-mesenchyme crosstalk in organ development. ACS Nano. 11(8):7736–7746.
Kallenbach E. 1978. Fine structure of the stratum intermedium, stellate reticulum, and outer enamel epithelium in the enamel organ of the kitten. J Anat. 126(Pt 2):247–260.
Lee MJ, Kim EJ, Otsu K, Harada H, Jung HS. 2016. Sox2 contributes to tooth development via Wnt signaling. Cell Tissue Res. 365(1):77–84.
Lesot H, Vonesch JL, Peterka M, Tureckova J, Peterkova R, Ruch JV. 1996. Mouse molar morphogenesis revisited by three-dimensional reconstruction: II. Spatial distribution of mitoses and apoptosis in cap to bell staged first and second upper molar teeth. Int J Dev Biol. 40(5):1017–1031.
Li J, Feng J, Liu Y, Ho TV, Grimes W, Ho HA, Park S, Wang S, Chai Y. 2015. BMP-SHH signaling network controls epithelial stem cell fate via regulation of its niche in the developing tooth. Dev Cell. 33(2):125–135.
Li L, Tang Q, Nakamura T, Suh JG, Ohshima H, Jung HS. 2016. Fine tuning of Rac1 and RhoA alters cuspal shapes by remolding the cellular geometry. Sci Rep. 6:37828.
Liu F, Millar SE. 2010. Wnt/β-catenin signaling in oral tissue development and disease. J Dent Res. 89(4):318–330.
Liu H, Yan X, Pandya M, Luan X, Diekwisch TG. 2016. Daughters of the enamel organ: development, fate, and function of the stratum intermedium, stellate reticulum, and outer enamel epithelium. Stem Cells Dev. 25(10):1580–1590.
Liu Y, Jin Y, Li J, Seto E, Kuo E, Yu W, Schwartz RJ, Blazo M, Zhang SL, Peng X. 2013. Inactivation of Cdc42 in neural crest cells causes craniofacial and cardiovascular morphogenesis defects. Dev Biol. 383(2):239–252.
Mao JJ, Prockop DJ. 2012. Stem cells in the face: tooth regeneration and beyond. Cell Stem Cell. 11(3):291–301.
Melendez J, Grogg M, Zheng Y. 2011. Signaling role of Cdc42 in regulating mammalian physiology. J Biol Chem. 286(4):2375–2381.
Modolo F, Biz MT, de Sousa SM, Fachinelli Rde L, Crema VO. 2012. Immunohistochemical expression of Rho GTPases in ameloblastomas. J Oral Pathol Med. 41(5):400–407.
O'Connell DJ, Ho JW, Mammoto T, Turbe-Doan A, O'Connell JT, Haseley PS, Koo S, Kamiya N, Ingber DE, Park PJ, et al. 2012. A Wnt-Bmp feedback circuit controls intertissue signaling dynamics in tooth organogenesis. Sci Signal. 5(206):ra4.
Olson MF, Ashworth A, Hall A. 1995. An essential role for Rho, Rac, and Cdc42 GTPases in cell-cycle progression through G(1). Science. 269(5228):1270–1272.
Peterkova R, Lesot H, Vonesch JL, Peterka M, Ruch JV. 1996. Mouse molar morphogenesis revisited by three dimensional reconstruction: I. Analysis of initial stages of the first upper molar development revealed two transient buds. Int J Dev Biol. 40(5):1009–1016.
Peters H, Balling R. 1999. Teeth: where and how to make them. Trends Genet. 15(2):59–65.
Regezi JA, Sciubba JJ, Jordan RC. 2016. Oral pathology: clinical-pathologic correlations. 7th ed. Amsterdam (Netherlands): Elsevier Health Sciences.
Rul W, Zugasti O, Roux P, Peyssonnaux C, Eychene A, Franke TF, Lenormand P, Fort P, Hibner U. 2002. Activation of ERK, controlled by Rac1 and Cdc42 via Akt, is required for anoikis. Ann N Y Acad Sci. 973:145–148.
Shigemura N, Kiyoshima T, Sakai T, Matsuo K, Momoi T, Yamaza H, Kobayashi I, Wada H, Akamine A, Sakai H. 2001. Localization of activated caspase-3-positive and apoptotic cells in the developing tooth germ of the mouse lower first molar. Histochem J. 33(5):253–258.
Thesleff I. 2014. Current understanding of the process of tooth formation: transfer from the laboratory to the clinic. Aust Dent J. 59 Suppl 1:48–54.
Thesleff I, Tummers M. 2008. Tooth organogenesis and regeneration. Cambridge (MA): Stembook.
Yang F, Zeng Q, Yu G, Li S, Wang CY. 2006. Wnt/beta-catenin signaling inhibits death receptor-mediated apoptosis and promotes invasive growth of HNSCC. Cell Signal. 18(5):679–687.
Yang JW, Zhu LX, Yuan GH, Chen YX, Zhang L, Zhang L, Chen Z. 2013. Autophagy appears during the development of the mouse lower first molar. Histochem Cell Biol. 139(1):109–118.
Zhang L, Yuan G, Liu H, Lin H, Wan C, Chen Z. 2012. Expression pattern of Sox2 during mouse tooth development. Gene Expr Patterns. 12(7–8):273–281.
Zhou C, Yang G, Chen M, Wang C, He L, Xiang L, Chen D, Ling J, Mao JJ. 2015. Lhx8 mediated Wnt and TGFβ pathways in tooth development and regeneration. Biomaterials. 63:35–46.